

**COMPREHENSIVE CONTROL FOR PV-BES MICROGRID ROOFTOP SOLAR AND ITS
EFFICIENT GRID SYNCHRONIZATION**

- U. Praveen**, UG Students, Sree Vahini Institute of Science and Technology (Autonomous),
Tiruvuru, Andhra Pradesh
- M. Anji Babu**, UG Students, Sree Vahini Institute of Science and Technology (Autonomous),
Tiruvuru, Andhra Pradesh
- T. Shiva Prasad**, UG Students, Sree Vahini Institute of Science and Technology (Autonomous),
Tiruvuru, Andhra Pradesh
- P. Naveen**, UG Students, Sree Vahini Institute of Science and Technology (Autonomous), Tiruvuru,
Andhra Pradesh
- K. Ramya**, Assist. Professor, Dept of EEE, Sree Vahini Institute of Science and Technology
(Autonomous), Tiruvuru.
- Dr. K. Kiran Kumar**, Assoc. Professor, Dept of EEE, Sree Vahini Institute of Science and
Technology (Autonomous), Tiruvuru.

ABSTRACT:

The objective of this effort is to synchronize a microgrid which uses solar photovoltaic's (SPV) and battery energy storage (BES) with the power grid. The system offers imbalanced load correction, frequency fluctuation reduction, power quality (PQ) enhancements, smooth synchronization between on-grid and off-grid modes of operation and operating under polluted grid situations. Utilising a solid-state transfer switch (SSTS), this system enables smooth transitions between on-grid and off-grid modes of operation by using a dual-third order generalized integrator-reduced order generalized integrator-frequency locked loop (dual-TOGI ROGI-FLL). In the on-grid mode, the VSC receives gating pulses from a current-controlled algorithm based on a TOGI-quadrature signal generator (TOGI-QSG). In the off-grid mode, an algorithm which is controlled by voltage is employed. The filtering capabilities of SOGI-FLL and DTOGI-ROGI-FLL under distorted grid settings are compared. The system performance is confirmed by satisfactory MATLAB simulation results under both dynamic and steady-state settings.

Keywords: SSTS, BDC, DTOGI-ROGI-FLL, TOGI-QSG, BES, polluted grid, synchronization and SPV array.

INTRODUCTION:

The threat posed by climate change to humanity has emerged. [1] outlines and explains some of the major factors. Fossil fuel combustion produces a significant portion of world emissions from the production of heat and power. Due to their blanket effect, these pollutants raise the global temperature. Renewable energy sources (RESs) have the ability to replace fossil fuel combustion in the current situation. Furthermore, in the first two years of this decade, 160 countries made their plans for sustainable energy from 2020 to 2030 public [2]. Worldwide, more than half of all power is used in residential and commercial buildings [3]. This market resulted in the rise in popularity of the distributed energy generation (DEG) idea, which has made it possible to integrate RESs on-site in such structures. The benefits of DEGs include increased power quality (PQ), decreased transmission costs and losses, increased usage efficiency, cost effectiveness, better dependability and assistance for peak shaving. When used in conjunction with a microgrid (MG), the DEGs can further increase the system dependability. As adaptable structures, MGs are able to deploy DEGs with control capability, meaning they can function independently and cut off from the electrical grid. Since most residential and commercial structures are concentrated in urban and suburban locations, there are significant restrictions on when the DEGs can be implemented.

Wind turbines with horizontal axes are avoided because they can become undesirables, impair the scenery and make noise. Although they can overcome these difficulties, vertical axis wind turbines

are in an infancy [4]. In urban and suburban settings, rooftop solar photo voltaic (SPVs) are a more feasible option for installing DEGs in buildings [5]. However, because the output from the SPV arrays is dependent on ambient temperature and solar radiation, an energy storage device is needed to satisfy load demands at night or during periods of low irradiation. Applications for battery energy storage (BES) in residential and commercial buildings offer increased dependability and a continuous power supply [6]. A number of variables affect the BES lifespan, but repeated cycles of charging and discharging have a major impact. Therefore, unwanted charging/discharging cycles should be removed in order to prevent the need to replace the BES on a regular basis. As a result, BES is only utilized to fulfill sporadic power demands when operating off the grid. The utility grid provides the unpredictable electricity while in on-grid mode. Temperature, sun shadowing, soiling, orientation, and operating point are some of the variables that affect the SPV array efficiency. For its optimum efficiency, the SPV must be running at the maximum power point (MPP) of the SPV array for a certain irradiation level, even if all other environmental factors are optimal. In a real-world situation, the amount of irradiance fluctuates constantly. As a result, the PV characteristics vary and each new P-V characteristic is its own maximum power point (MPP). As the irradiation changes, the operational point of the SPV array must continuously monitor this point. Therefore, in order to monitor the MPP quickly and precisely, an MPP tracking (MPPT) algorithm is required. The needs is being achieved by a variety of methods, including fuzzy logic, incremental conductance and perturb and observe (P&O) [7]. In this paper, an enhanced P&O algorithm is employed [8]. This control technique eliminates drift when tracking the MPP, in contrast to the conventional P&O algorithm.

A solid-state transfer switch (SSTS) and a synchronization control are used to synchronize the MG grid. The synchronization control checks the synchronization conditions and then sends a "high" or "low" signal to the SSTS. Due to variations in the power flow, transients in voltages and currents occur when the MG switches between off-grid and on-grid modes of operation. Abrupt changes in the reference voltages and currents generation can also cause frequency discrepancies. As a result, the MG's control strategy needs to be able to handle these circumstances and provide smooth grid synchronization. Phase-locked loops (PLLs) are typically employed to identify the synchronization control parameters. Frequency locked loops, or FLLs, are utilized since PLLs operate weakly under dynamic settings because to overshoots [9]. Dual-third order generalized integrator-reduced order generalized integrator-FLL (DTOGI-ROGI-FLL) is used in this study.

For filtering the higher-order harmonics from the contaminated grid voltages, the DTOGI-ROGI FLL serves to reduce the pollution of the grid. In the event of a deformed grid, the third-order filter outperforms the second-order filter [10]. PQ problems arise from the use of power electrical components in the MG functioning. The shunt-connected voltage source converter (VSC), which functions as a distribution static compensator (DSTATCOM) in conjunction with the DC link, is used to alleviate the PQ problems. The control algorithms for the VSC were proposed in several tries. Traditional adaptive algorithms which are implemented under dynamic settings, such as least mean square (LMS), variable step size-LMS (VSS-LMS), and least mean fourth (LMF), perform poorly [11]. Poor harmonic rejection capability and DC-offset rejection capability are problems with controllers from the second order generalized integrator frequency locked loop (SOGI-FLL) and modified versions of SOGI-FLL. As a result, a third-order filter is employed to enhance the control selectivity and offer even greater attenuation to higher-order harmonic components than modified second-order filters. These are several of the paper emphasizes:

1. An enhanced P&O MPPT control is used to capture the solar PV array peak power as shown by the P-V curve.
2. In off-grid mode, BES improves system dependability by counteracting power intermittency.
3. An STS, synchronization control, and DTOGI-ROGI-FLL are used to achieve smooth mode-transfer operations across the various modes.
4. DTOGI-ROGI-FLL is used to handle the operation under contaminated grid situations.
5. VSC control is used to improve PQ, including power factor (PF) enhancement, harmonic

reduction, and unbalanced loading adjustment. In the off-grid mode, a voltage-based control is employed, whereas in the on-grid mode, a TOGI-QSG-based control is employed.

SYSTEM DESIGN:

The structure of the MG under investigation in this paper is shown in Fig. 1. A three-leg VSC, local loads, RC ripple filters, an SSTS, a BES, a BDC, an SPV array and a three-phase grid comprise this system. Typical inductive and resistive loads represent the local loads, which are interfaced to the PCC by means of non-linear components as a full-bridge diode rectifier. RC filters are used to filter the higher order frequency ripples from grid voltages and PCC. The current ripples are handled by the interacting inductors. A BDC is used to integrate the BES into the DC connection. The BDC handles the BES charging and draining in addition to controlling the DC link voltage to the MPP level.

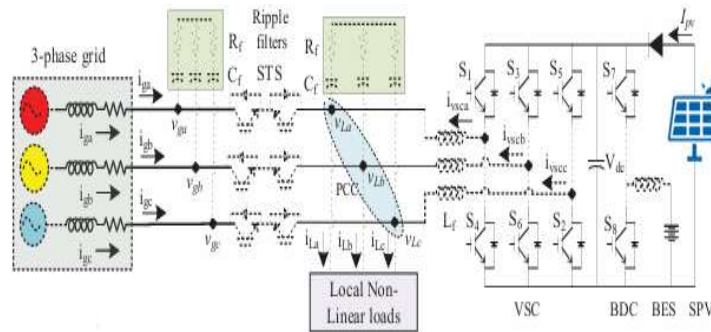


Fig.1. System architecture

CONTROL STRATEGY:

This study included four control strategies as part of its control plan for a single-stage SPV-BES-based MG. The following are a few illustrations of the control methods: During system dynamics, this control minimized drift in tracking the MPP. When the PV power and PV voltage at the nth instant are compared to the (n-1)th instant, it operates by following the flowchart in Fig. 2.

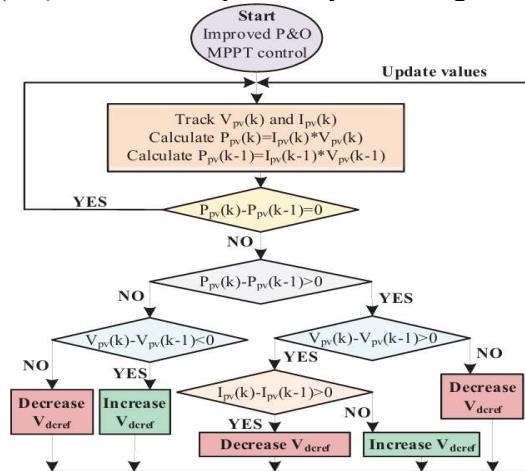


Fig. 2: Superior control of P&O MPPT

CONTROL OF VSC :

For the VSC to execute inversion operations and PQ improvements, the switches it uses must be controlled by an intelligent control algorithm. In the on-grid mode of operation, the gating pulses are generated through a current-controlled algorithm based on TOGI-QSG [12]. An algorithm which is regulated by voltage is employed when operating off the grid. The circuit senses the following parameters: load currents (iLa, iLb, iLc), grid currents (iga, igb, igc), PV voltage and PV current

(V_{pv}, I_{pv}) and line grid voltages (v_{gab}, v_{gbc}). The following parts include the VSC control for various modes:

On-Grid Mode

The on-grid mode of operation control method is depicted in Fig. 3. In the on-grid mode of operation, the utility grid, local loads and the SPV array exchange power while the BES functions in a floating mode. The following categories can be used to separate the computation used to generate gating pulses:

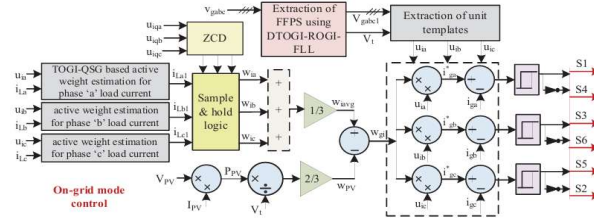


Fig. 3 On-grid mode VSC control.

CALCULATION OF UNIT TEMPLATES:

A sinusoidal signal with a unit amplitude serves as the unit template, which is computed to record the grid phase voltages phase angle. For this reason, in order to keep the grid side unity power factor (UPF), the reference grid currents are generated in the same phase as the grid voltages. Using detected line-line voltages (v_{ab}, v_{bc}), the phase voltages are calculated.

$$v_a = \frac{2v_{ab} + v_{bc}}{3}, v_b = \frac{-v_{ab} + v_{bc}}{3}, v_c = \frac{-v_{ab} - 2v_{bc}}{3} \quad (1)$$

The grid phase voltages amplitude can be determined as follows:

$$V_t = \sqrt{\frac{2}{3}(v_{ga1}^2 + v_{gb1}^2 + v_{gc1}^2)} \quad (2)$$

The quadrature and in-phase unit templates are acquired as follows:

$$u_{ia} = \frac{v_{ga1}}{V_t}, u_{ib} = \frac{v_{gb1}}{V_t}, u_{ic} = \frac{v_{gc1}}{V_t} \quad (3)$$

$$u_{qa} = -\frac{u_{ia}}{\sqrt{3}} + \frac{u_{ic}}{\sqrt{3}}, u_{qb} = \frac{\sqrt{3}}{2}u_{ia} + \frac{u_{ib}}{2\sqrt{3}} - \frac{u_{ic}}{2\sqrt{3}}, u_{qc} = -\frac{\sqrt{3}}{2}u_{ia} + \frac{u_{ib}}{2\sqrt{3}} - \frac{u_{ic}}{2\sqrt{3}} \quad (4)$$

Utility grid voltages are typically assumed to be sinusoidal and harmonic-free, although load non-linearities can cause distortion. The fundamental frequency positive sequence (FFPS) voltages (v_{ga1}, v_{gb1} and v_{gc1}) are therefore extracted from the distorted grid voltages by Dual-TOGI-ROGI-FLL, as seen in Fig. 4. When calculating FFPS in the unit template, gating pulses are generated correctly and polluted grid conditions are lessened.

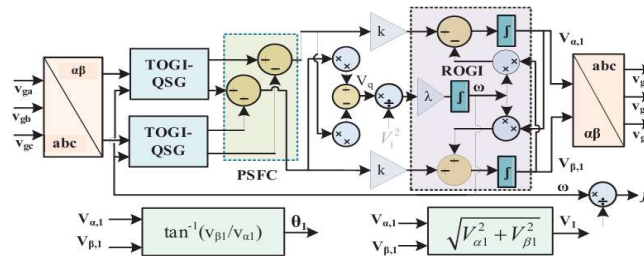


Fig. 4 Structure of DTOGI-ROGI-FLL

PV FEED-FORWARD ESTIMATION :

When PV feed-forward is used, the grid current is rapidly changed, improving the system dynamic responsiveness to changing solar irradiation and SPV array outages and reconnects. The SPV feed-forward may be computed as follows:

$$w_{pv}(n) = \frac{2P_{pv}(n)}{3V_t} \quad (5)$$

Where Ppv is harvested power from the SPV array.

ESTIMATION OF FUNDAMENTAL WEIGHT OF LOAD CURRENTS:

TOGI-QSG is used to extract the basic components of the load currents (i_{la1} , i_{lb1} , i_{lc1}) from detected load currents (i_{La} , i_{Lb} , i_{Lc}). Fig. 5 shows the structure of the TOGI-QSG. The output y_d is the essential component of the load current of the corresponding phase, whereas the input "u" represents the input signal as perceived load current. A sample and hold logic receive the fundamental load current, as shown in Fig. 3. The quadrature unit templates zero crossings initiate the sample and hold logic. The sample and hold logic output are used to determine the weight components of the load current.

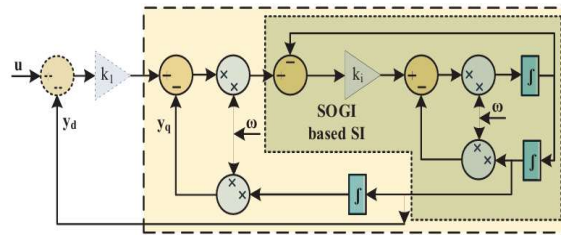


Fig. 5 Structure of TOGI-QSG

REFERENCE CURRENTS CALCULATION:

The active weight components of each of the three phases produced at the sample and hold circuits output are averaged in order to provide balanced grid currents:

$$w_{iavg} = \frac{(w_{ia} + w_{ib} + w_{ic})}{3} \quad (6)$$

The component of net active weight is calculated as follows:

$$w_{gi} = w_{iavg} - w_{pv} \quad (7)$$

The reference grid current of phase "x" is calculated by multiplying the net active weight component by the corresponding phase in-phase unit templates.

$$i_{ga}^* = w_{gi}^* u_{ia}, i_{gb}^* = w_{gi}^* u_{ib}, i_{gc}^* = w_{gi}^* u_{ic} \quad (8)$$

GATING PULSES FOR VSC:

The hysteresis current controller receives the detected grid currents (i_{ga} , i_{gb} , i_{gc}) and the reference grid currents (i_{ga}^* , i_{gb}^* , i_{gc}^*). For generating the switching pulses necessary for the VSC to function, the hysteresis current controller (HCC) controls the error between the currents within the pre-established hysteresis range.

Off-Grid Mode

The control algorithm utilized in the off-grid mode of operation is shown in Fig. 6.

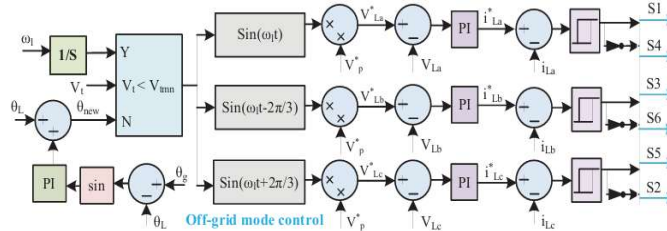


Fig. 6 Off-grid mode VSC control

When operating in this mode, the BES serves as the main backup source. After the load requirement is fulfilled, the BES receives the extra PV electricity. In order to address power intermittency on cloudy days, at night, or even during periods of high loading when the PV power is not enough to

fulfill the load demand, the BES is utilized. It describes where the reference load phase voltages (v_{La}^* , v_{Lb}^* and v_{Lc}^*) are produced:

$$v_{La}^* = V_p^* \sin(\omega_l t), v_{Lb}^* = V_p^* \sin(\omega_l t - \frac{2\pi}{3}), v_{Lc}^* = V_p^* \sin(\omega_l t + \frac{2\pi}{3}) \quad (9)$$

where V_p^* is the reference voltage amplitude and ω_l is the angular frequency. Real line-line load voltages are used to determine the load phase voltages. An error signal is then produced and delivered to a PI controller (PIC) through comparison of the reference load phase voltages with the actual load phase voltages (v_{La} , v_{Lb} , and v_{Lc}) in real time. The error signal is produced by the PIC as reference load currents (i_{La}^* , i_{Lb}^* , and i_{Lc}^*). The error signal is transmitted to HCCs where it gets compared with the actual load current (i_{La} , i_{Lb} , and i_{Lc}) in real time. The pre-established hysteresis bands are used by the HCCs to create the gating pulses. When the VSC is operating off the grid, these pulses regulate the switches which are used.

SYNCHRONIZATION ALGORITHM:

The demands are generated for the synchronization algorithm. For each of the three synchronization criteria, the algorithm considers. Phase angle inaccuracy, grid frequency, and grid voltage magnitude are therefore subject to the circumstances. The magnitude of the grid voltage needs to be within the allowed range. Reducing the phase angle error to a predetermined limit requires that the load phase angle synchronize with the grid phase angle. The grid frequency required to fall within the 1% error range. When every criterion is met, the SS signal changes to "1," or "high," or "0," or "low."

$$SS = \begin{cases} 1, & GC \text{ mode, when } \left\{ \begin{array}{l} V_{r_{min}} \leq V_r \leq V_{r_{max}} \\ f_{g_{min}} \leq f_g \leq f_{g_{max}} \\ \Delta\theta_{min} \leq \Delta\theta \leq \Delta\theta_{max} \end{array} \right\} \\ 0, & SA \text{ mode, otherwise} \end{cases} \quad (10)$$

The DTOGI-ROGI-FLL generates the grid phase (θ_g), load phase (θ_L) and grid frequency.

BDC Control

In Fig. 7, the BDC control is shown. Switching pulses for switches S7 and S8 are produced by the BDC control. As the design employed there integrates the SPV array to the DC link in a single stage, the BDC is responsible for regulating the DC link voltage at the same level as the MPP voltage of the SPV array. Consequently, in the BDC control, the reference DC link voltage ($V_{dc_{ref}}$) equals the monitored MPP voltage.

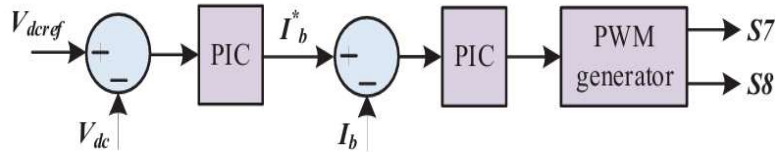


Fig. 7 BDC control

The setup utilizes the flexibility of a cascaded PIC. The error between the real-time DC link voltage and the reference DC link voltage is transmitted to the outer PIC. BES current reference is the output. The inner PIC and a PWM generator receive the difference between the reference and real-time BES currents. Gating pulses are generated by the PWM generator. In accordance with the system, the PIC gains are appropriately adjusted.

SIMULATION RESULTS :

The solar PV-BES-based MG is simulated using MATLAB/Simulink, and the effectiveness of the proposed control technique is studied. The results obtained under different circumstances are discussed in the following sections.

DYNAMIC RESPONSE TO SPV CHANGES:

The system dynamic performance during changes at the SPV array is shown in Fig. 8. The SPV array is initially operational and operating at an irradiation intensity of 1000 W/m². Non-linear currents,

shown as iload in Fig. 8, are drawn by the 4.1 kW non-linear loads connected at the PCC. The load currents are polluted by higher-order harmonics, which are compensated for by the VSC current (i_{VSC}). The collected SPV power (P_{pv}) at 1000 W/m² is 6.24 kW. The extra PV is sent into the grid when the load demand has been satisfied. The P_{pv} drops to 1.85 kW at 0.34 s when the solar irradiation intensity drops to 300 W/m². The utility grid now supplies sporadic electricity since the collected PV is no longer enough to fulfill the load requirement. As a result, the grid power flow is inverted, which causes the grid currents to flow in the other form. The generation from the SPV array is now totally decreased at 0.38s. As a result, the electric grid now provides all of the demand. Nonetheless, the resilience of the system is shown, as neither current nor voltage transients occur. The SPV array resumes power generation at an irradiation intensity of 300 W/m² at 0.42 seconds. Only a periodic demand for power is now supplied by the system. As a result, the grid current decreases. With 1000 W/m² of solar energy, the system returns to its starting condition within 0.46 seconds. V_{dc} , the DC link voltage, is kept constant.

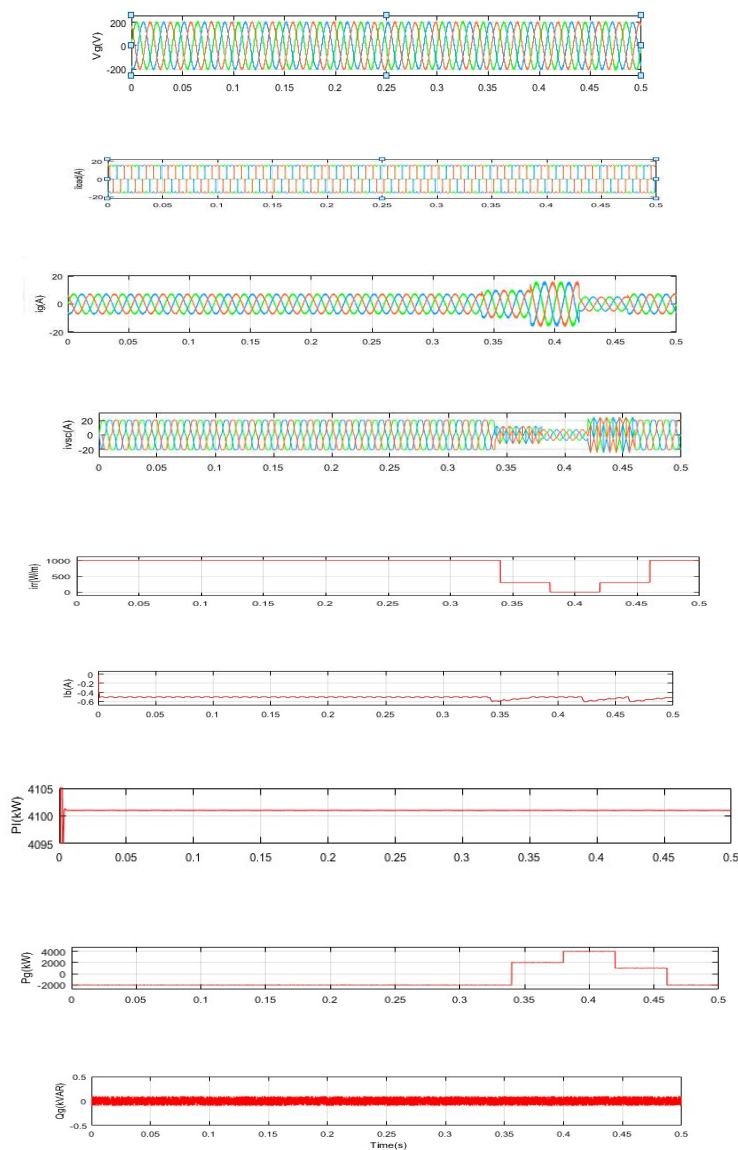


Fig. 8 Dynamic performance during varying irradiancies

DYNAMIC PERFORMANCE UNDER UNBALANCED LOADING CONDITIONS :

The dynamic performance of the system under imbalanced loads in the on-grid mode of operation is depicted in Fig. 9. The SPV array runs at an irradiation level of 1000 W/m² and 4.1 kW non-linear loads are connected. A circuit breaker is used to separate the loads connected at phase "c" from the system because of a malfunction in the load terminal of that phase. As a result, the remaining loads linked at phases "a" and "b" seem to be single-phase loads connected in series. When the phase "c" load current weight component falls to zero, the average weight component also falls. Furthermore, the load current waveform shown in Fig. 9 shows the impacts. In accordance with IEEE 519, the VSC currents maintain sinusoidal grid currents by compensating for this anomaly on the load side. The injected grid power/current increases as the load demand decreases. BDC is used to maintain the V_{dc} constant.

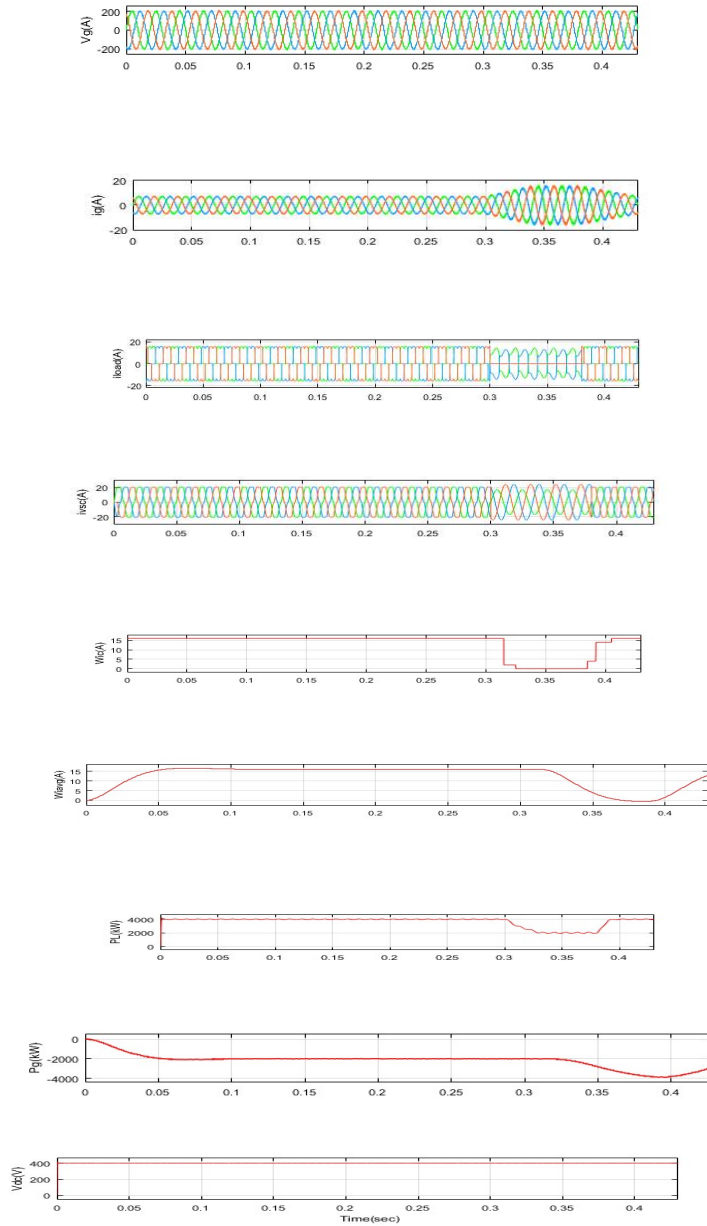


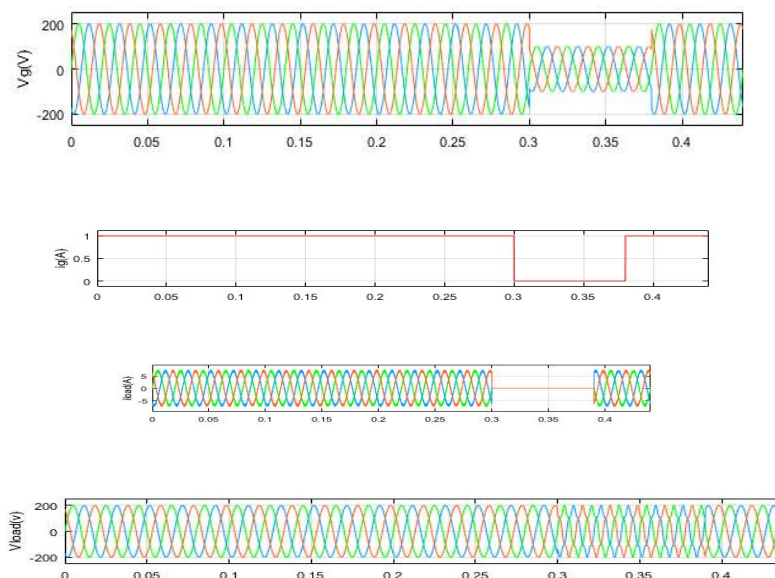
Fig. 9 Dynamic performance on unbalanced loading

PERFORMANCE AT DISTORTED GRID :

The system performance under distorted grid circumstances is shown in Fig. 10. The 5th harmonic components, which predominate between 0.2 and 0.28 seconds, alter the grid voltages. The creation of inaccurate reference grid currents would result from creating unit templates from the distorted voltages. In order to phase out this state, DTOGI-ROGI-FLL isolates the fundamental grid voltages (v_{g1}) from the distorted one. Fig. 10(a) shows the unpolluted unit templates that were produced as uTOGI. According to IEEE 519, the resulting grid currents are sinusoidal. Fig. 10(b) illustrates the extraction of the fundamental grid voltages and the grid currents using SOGI-FLL in order to evaluate the proposed control's polluted grid mitigation capabilities with that of traditional SOGI-FLL control. The harmonic spectra of the contaminated grid voltages are shown in Fig. 11(a). Using DTOGI ROGI-FLL, the harmonic spectra of the basic grid voltages and currents are displayed in Figs. 11(b)–(c). Using SOGI-FLL, the harmonic spectra of the basic grid voltages and currents are displayed in Figs. 11(d)–(e). Compared to 2.5% when utilizing SOGI-FLL, the THD of the basic grid voltages retrieved by DTOGI ROGI-FLL is significantly reduced at 0.88%. As a result, grid currents employing DTOGI-ROGI-FLL have a THD of 3.59%, whereas SOGI-FLL has a THD of 4.06%. Consequently, DTOGI-ROGI-FLL demonstrates improved harmonic rejection capacity in distorted grid conditions.

MODE SHIFT OPERATIONS:

The mode shift procedures between the off-grid and on-grid modes. At first, the synchronization control three requirements are achieved. Consequently, the MG is functioning in an on-grid mode and the SS signal is strong. In floating mode, the BES is functioning. The grid voltage level is now reduced from 1 p.u. to 0.5 p.u. at 0.3s. As a result, the SS signal becomes "low" and the synchronization control voltage magnitude condition is fulfilled. Additionally, the VSC control transitions to the voltage-controlled operation mode and the SSTS is opened. The MG is now operating in off-grid mode. The BES is currently where the extra Ppv is maintained. The load current is being reproduced by the VSC current. The grid voltages are restored to 1 p.u. at 0.38 seconds. However, the synchronization criteria must be satisfied in half a cycle. The STS is closed when the SS signal becomes "high." Synchronization is accomplished when the VSC control also transitions to the current-controlled mode of operation. The BES begins to function in a floating mode when the grid begins to absorb the extra PV. Throughout the procedures, the V_{dc} remains constant.



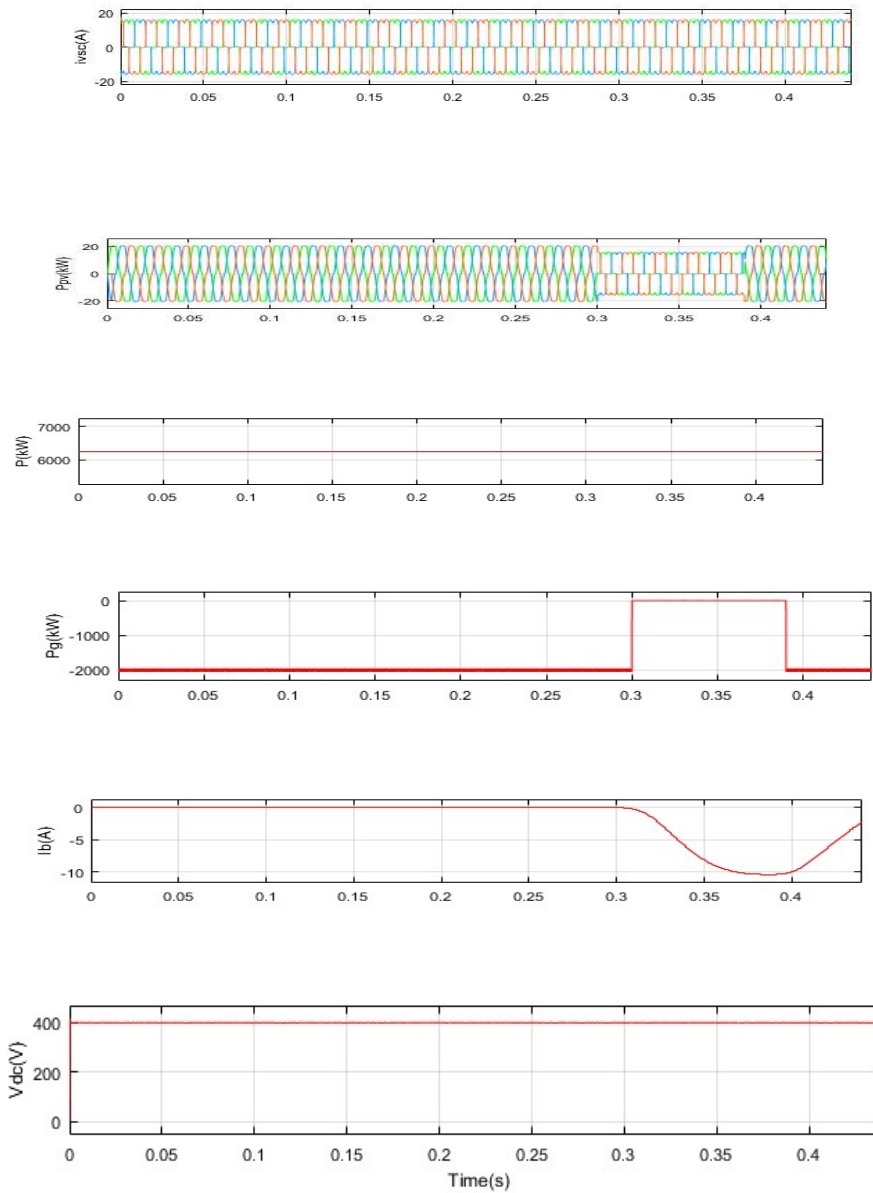


Fig. 10 Mode shift operation to GI mode from SA mode

CONCLUSION:

The proposed control technique is used to develop and simulate a single-stage SPV-BES-based MG in order to evaluate the system performance under both steady-state and different dynamic situations. The DC link voltage must correspond to the SPV array MPP voltage in order to use the single-stage arrangement. Therefore, in contrast to the traditional P&O algorithm, an enhanced P&O algorithm performs the task and removes drift in tracking the MPP point. As a result, BDC more precisely balances the DC link voltage. The VSC switches receive switching pulses from the VSC control. The on-grid mode of operation is regulated using a current-controlled technique based on TOGI-QSG, whereas the off-grid mode is controlled by a voltage-controlled technique. Synchronization control uses DTOGI-ROGI-FLL to extract the relevant parameters (grid frequency, grid, and load phase angle) from the grid voltages and load voltages and verifies for the circumstances required for

synchronization. For eliminating the higher order grid voltages from the polluted grid voltages, DTOGI-ROGI-FLL also effectively controls polluted grid circumstances. The use of DTOGI-ROGI-FLL and SOGI-FLL for dirty grid adjustment is compared. By using buck and boost modes of operation, the BDC control regulates the BES charging and discharging functions. The simulation results show that the control technique performs well in both dynamic and steady-state circumstances. According to IEEE-519 and IEEE-1547 standards, the THDs of load voltages and grid currents are restricted to about 5%.

REFERENCES:

- [1] Sixth Assessment Report, Climate Change 2022: Impacts, Adaptation and Vulnerability. Intergovernmental Panel on Climate Change (IPCC) February 2022.
- [2] High-level Dialogue on Energy, UN-energy Press release, New York, September 2021.
- [3] M. González-Torres, L. Pérez-Lombard, Juan F. Coronel, Ismael R. Maestre and Da Yan, "A review on buildings energy information: Trends, end-uses, fuels and drivers, Energy Reports," vol. 8, pp. 626- 637, ISSN 2352-4847, 2022.
- [4] R. Kumar, K. Raahemifar and A. S. Fung, "A critical review of vertical axis wind turbines for urban applications," Renewable and Sustainable Energy Reviews, 2018.
- [5] K. Sunderland, M. Narayana, G. Putrus and M. Conlon, "Levelized cost of energy analysis: A comparison of urban (micro) wind turbines and solar PV systems," 51st International Universities Power Engineering Conference (UPEC), pp. 1-6, 2016.
- [6] W. De Carvalho, E. L. Ratnam, L. Blackhall and A. Von Meier, "Optimization-based operation of distribution grids with residential battery storage: Assessing utility and customer benefits," IEEE Transactions on Power Systems, Early Access.
- [7] R. B. Bollipo, S. Mikkili and P. K. Bonthagorla, "Hybrid, optimal, intelligent and classical PV MPPT techniques: A review," CSEE Journal of Power and Energy Systems, vol. 7, no. 1, pp. 9-33, 2021.
- [8] A. K. Singh, I. Hussain and B. Singh, "An improved adaptive P&O technique for two stage grids interfaced SPVECS," IEEE International Conference on Industrial Electronics for Sustainable Energy Systems (IESES), pp. 320-325, 2018.
- [9] S. Golestan, J. M. Guerrero and J. C. Vasquez, "High-order frequency-locked loops: A critical analysis," IEEE Transactions on Power Electronics, vol. 32, no. 5, pp. 3285-3291, May 2017.
- [10] T. Ngo and T. Vu, "Comparative study of the second-order and thirdorder systems for the synchronization system under distorted grid conditions," IEEE Power & Energy Society General Meeting (PESGM), pp. 1-5, 2019.
- [11] A. Parida and B. Subudhi, "A variable step size robust least mean logarithmic square-based control scheme for improved power quality of grid-interfaced PV system," IEEE Transactions on Smart Grid, vol. 13, no. 3, pp. 2086-2093, May 2022.
- [12] J. Fang, S. Yang, Z. Xie and L. Wang, "Enhanced frequency-locked loop based on a third-order generalized integrator," IEEE 12th International Symposium on Power Electronics for Distributed Generation Systems (PEDG), pp. 1-8, 2021.